Available online at www.sciencedirect.com

SciVerse ScienceDirect

Geochimica et Cosmochimica Acta 117 (2013) 115–128

Geochimica et Cosmochimica Acta

www.elsevier.com/locate/gca

An atomic force microscopy study of the dissolution of calcite in the presence of phosphate ions

J. Klasa [a,b], E. Ruiz-Agudo [c,*], L.J. Wang [d], C.V. Putnis [a], E. Valsami-Jones [b,e], M. Menneken [a], A. Putnis [a]

[a] Institut für Mineralogie, University of Münster, Corrensstrasse 24, 48149 Münster, Germany
[b] Department of Earth Sciences, Natural History Museum, Cromwell Road, SW7 5BD London, UK
[c] Department of Mineralogy and Petrology, University of Granada, Fuentenueva s/n, 18071 Granada, Spain
[d] College of Resources and Environment, Huazhong Agricultural University, Wuhan, Hubei 430070, China
[e] School of Geography, Earth & Environmental Sciences, University of Birmingham, Edgbaston B15 2TT, UK

Received 7 June 2012; accepted in revised form 20 March 2013; available online 8 April 2013

Abstract

Dissolution of calcite in the presence of phosphate solutions was studied *in situ* by Atomic Force Microscopy. Results of experiments in slightly alkaline $(NH_4)_2HPO_4$ solutions showed that dissolution, measured from etch pit spreading, is significantly reduced compared to that observed in pure deionized water, confirming an inhibitory effect of $(NH_4)_2HPO_4$ on calcite dissolution. However, rates measured in the presence of Na-phosphate solutions at the same pH remained close to that in pure water. This would indicate that the inhibitory effect could be caused by the presence of the NH_4^+ group. Moreover, for phosphate solution concentrations >5 mM, the precipitation of a calcium phosphate phase occurred simultaneously while calcite was dissolving, despite the continuous flow of the reaction solution. Such reactions may play an important role in phosphorus recovery from P-bearing solutions. Importantly this study gives insights into the mechanism of interface-coupled dissolution-precipitation reactions occurring during the interaction of phosphate-bearing solutions with calcium carbonate minerals and emphasizes the importance of performing direct observations when determining the kinetics of dissolution reactions, as they can be significantly affected by the precipitation of secondary phases that could alter dissolution rates determined from measurements of bulk solution composition.

1. INTRODUCTION

Mineral–fluid interactions have recently gained interest in many research fields due to the recognition of the extensive role of aqueous fluids in geochemical processes in the Earth's crust. Fluids are essential for surface weathering as well as in the control of deep Earth processes such as metasomatism and metamorphism (Lee et al., 2008; Putnis, 2009; Jamtveit and Austrheim, 2010; Putnis and Austrheim, 2010) and consequently for the mobilization of elements within the Earth. Thus, a sound knowledge of the mechanisms controlling fluid-surface interactions is necessary for understanding important large-scale Earth processes (Putnis and John, 2010). Moreover, fluids are necessary for many biological systems as the medium for element transport such as ion transport across cell membranes in plants (Schachtmann et al., 1998) or transport of ions through protein channels in animal cells (Ren et al., 2001). Aqueous fluids also have implications in engineering applications such as the preservation of built cultural heritage (Ruiz-Agudo et al., 2007), prevention or control of

* Corresponding author.
E-mail addresses: j_klasa03@uni-muenster.de (J. Klasa), encaruiz@ugr.es (E. Ruiz-Agudo), ljwang@mail.hzau.edu.cn (L.J. Wang), putnisc@uni-muenster.de (C.V. Putnis), e.valsami-jones@nhm.ac.uk (E. Valsami-Jones), m_menn@uni-muenster.de (M. Menneken), putnis@uni-muenster.de (A. Putnis).

0016-7037/$ - see front matter © 2013 Elsevier Ltd. All rights reserved.
http://dx.doi.org/10.1016/j.gca.2013.03.025

scale-forming minerals in industrial processes, such as calcite and barite blocking of oil wells and reservoirs (Putnis et al., 2008), or in the design of non corrosive materials for orthopaedic applications (Jacobs et al., 1998).

Calcite and carbonate minerals are major minerals in the Earth's crust, comprising approximately 20% of the surface sedimentary rocks. Understanding the mechanisms of their dissolution is essential for the modeling of geochemical cycles (Morse and Arvidson, 2002) and more recently for modeling systems for CO_2 storage (Stockmann et al., 2011).

Phosphorus (P) is a component of proteins and is therefore essential for life. P availability for plant uptake is the first step in the biogeochemical cycling of P. It was the introduction of phosphate fertilizers that greatly enhanced crop production in the early 20th century. However the excessive use of P-rich fertilizers results in high phosphorous concentrations both in soils and surface water runoff. These agricultural additions of phosphates inevitably find their way into surface drainage systems and eventually to the oceans, causing marine coastal 'dead zones' enriched in algae. Phosphates are also very important in many manufacturing industries including detergents and cleaning agents, food and drink additives. Therefore, phosphates represent a significant contribution to anthropogenic waste, with only 10% of the total phosphorous being recycled. This imbalance between phosphorus loss and phosphorus being recovered, as well as its limited resources, significantly affects phosphate sustainability (Elser and Bennett, 2011).

Given the ubiquitous occurrence of carbonate minerals in the Earth, as well as the importance of phosphates in aqueous systems, a study of the interaction between phosphate solutions and calcite surfaces is timely both for an understanding of the reaction mechanism as well as an attempt to elucidate possible remediation of high concentrations of phosphates in rivers, lakes, ground water and the oceans. Previous research has shown that carbonates may be used for phosphate sequestration (Karageorgiou et al., 2007). Furthermore, as carbonates are common constituents of sediments and soils, their reaction with phosphate-containing aqueous solutions limits the availability of P for plant growth. Effectively this means that calcite – phosphate reactions may have a significant control on the flux of P within the superficial Earth and biological environments (Sø et al., 2011; Wang et al., 2012a,b).

In the present study, Atomic Force Microscopy (AFM) has been used to observe and quantify the kinetics of the reactions occurring at the calcite surface during contact with phosphate-containing solutions. AFM has the advantage of enabling the visualization of surface features in real time and at atomic scale resolution. A fluid cell coupled to the AFM has been used to observe *in situ* interactions of solutions containing phosphate ions, at various concentrations, with calcite surfaces. The aim of this study is to attempt to understand the mechanism of calcite dissolution in the presence of solutions containing phosphate ions.

2. EXPERIMENTAL PROCEDURE

In situ dissolution experiments were performed using a Multimode and D3000 AFM (Digital Instruments, Bruker) working in contact mode and equipped with a fluid cell. Before each experiment a rhombohedral calcite crystal of optical quality Iceland Spar (Chihuahua, Mexico) was cleaved with a blade in order to expose a fresh $\{10\bar{1}4\}$ cleavage surface. Cleavage rhombs of ca. $4 \times 3 \times 1$ mm in size were mounted in the fluid cell holder (Multimode AFM fluid cell volume 50 μL, fluid volume ca. 38 μL). Solutions were passed through the fluid cell using syringes attached to inlet and outlet tubes. All experiments were performed under ambient conditions (22 °C and partial pressure CO_2 $\sim 10^{-3.5}$ atm.). The influence of a range of phosphate concentrations (5×10^{-7} M to 1 M) was tested. Solution concentrations and pH values are given in Table 1. The phosphate salts used were: di-ammonium hydrogenphosphate $(NH_4)_2HPO_4$, (pH ~8), disodium hydrogenphosphate Na_2HPO_4 (pH ~8), and sodium di-hydrogen phosphate NaH_2PO_4 (pH ~4–5), Additionally $MgCl_2$ and NaCl at 0.1 M concentration were added to $(NH_4)_2HPO_4$ solutions to study the effect on dissolution at increased ionic strength (IS). Solutions were prepared from high-purity solids, $(NH_4)_2HPO_4$, NaH_2PO_4, Na_2HPO_4, NaCl, $MgCl_2$ (Aldrich) dissolved in deionized water (resistivity >18 mΩ cm^{-1}). The chemical speciation of each solution was determined using the PHREEQC software (Parkhurst and Appelo, 1999). The saturation state of the solution with respect to solid phases is given by the saturation index (SI):

$$SI = \log \Omega = \log(IAP/K_{sp})$$

where Ω is the supersaturation, IAP is the Ion Activity Product and K_{sp} the solubility product. All experimental solutions were prepared immediately prior to each experiment and were initially undersaturated with respect to any possible solid phase. Each of the solutions was gradually passed over the calcite surface at a constant flow rate ca. 50 mL h^{-1}. The chosen flow rate was sufficient to ensure surface-controlled reaction and not diffusion reaction in accordance with many previous AFM experiments (Liang and Baer, 1997).

Experiments were repeated at least twice to ensure reproducibility of the results. The PHREEQC (Parkhurst and Appelo, 1999) program was used to model the evolution of solution compositions during the hypothetical batch dissolution reactions of calcite in 38 μL of phosphate-bearing solutions. This reaction was simulated via the addition of small increments of $CaCO_3$ (500 steps) to the solution until equilibrium with respect to calcite was reached. As well, the SI of each solution with respect to the different calcium phosphate (Ca-P) phases was calculated at the last step (i.e. when the solution was in equilibrium with respect to calcite) of the dissolution reaction.

The AFM images were analyzed using the NanoScope software (Version 5.12b48). The scanning frequency was ca. 3 Hz with an average scan time of 1.5 min per scan, and areas scanned were typically 10×10 μm and 5×5 μm, although larger scans were also performed to check for possible tip influence on the scanned area. Summed step-edge migration velocities (Lea et al., 2001), or etch pit spreading rates, during dissolution were determined for each concentration of phosphate solution. Measurements of the length of shallow (one unit cell, approx

Table 1
Measured and calculated pH values and theoretical maximum calcium concentration in the tested phosphate solutions in equilibrium with calcite. Note: the discrepancy between measured and calculated pH at lower concentrations is probably due to the difficulty in correctly measuring solutions containing very few ions. Calculations made using PHREEQC (Parkhurst and Appelo, 1999).

Concentration of phosphate	$(NH_4)_2HPO_4$			Na_2HPO_4			NaH_2PO_4		
[mM]	$^{Total}Ca$[a] [M]	pH[b]	pH[c]	$^{Total}Ca$[a] [M]	pH[b]	pH[c]	$^{Total}Ca$[a] [M]	pH[b]	pH[c]
0.0005	1.27E−04	5.6	7.3	1.22E−04	8.2	7.3	1.22E−04	5.5	6.7
0.001	1.23E−04	5.6	7.5	1.22E−04	8.2	7.5	1.23E−04	5.4	6.6
0.005	1.27E−04	5.8	7.8	1.24E−04	8.3	7.9	1.26E−04	5.3	6.3
0.01	1.31E−04	5.6	7.9	1.26E−04	8.2	8.1	2.58E−04	5.3	6.1
0.1	2.18E−04	6.5	8.0	1.56E−04	8.2	8.5	1.97E−04	5.3	5.6
0.5	5.34E−04	6.8	8.0	2.54E−04	8.1	8.9	5.60E−04	4.9	5.3
1	8.36E−04	7.5	8.0	3.36E−04	8.2	9.0	9.89E−04	4.8	5.1
5	2.45E−03	7.7	8.0	6.94E−04	8.0	9.3	3.34E−03	5.4	4.8
10	3.97E−03	7.9	8.0	9.48E−04	8.0	9.3	5.26E−03	4.6	4.7
50	1.34E−02[d]	7.9	7.9	1.98E−03[d]	8.0	9.2	1.51E−02[d]	4.6	4.5
100	2.38E−02[d]	7.9	7.9	2.63E−03[d]	8.0	9.1	2.41E−02[d]	4.5	4.5
500	1.15E−01[d]	8.0	7.9	7.31E−03[d]	8.0	8.8	7.46E−02[d]	4.2	4.3
1000	2.72E−01[d]	8.1	8.0	1.11E−02[d]	8.0	8.7	1.21E−01[d]	4.0	4.2

[a] Total concentration of Ca calculated using phreeqc.dat.
[b] Measured pH.
[c] Calculated pH (using PHREEQC).
[d] Total concentration of Ca calculated using Wateq4f.dat.

3 Å deep) etch pits, as a function of time, were collected from sequential images scanned in the same direction. At least six etch pits in three sequential images were measured for each given solution concentration (see Ruiz-Agudo and Putnis (2012) for a recent review of direct observations of mineral–fluid reactions using AFM: the specific example of calcite).

Inductively coupled plasma optical emission spectrometry ICP-OES (Atom Scan Thermo Jarrell Ash) was used for determining the calcium concentration of 5 mL aliquots collected after flowing each concentration of $(NH_4)_2HPO_4$ solution over a calcite surface. Each 5 mL of solution flowed over the surface for approx. 6 min. After the AFM experiments several calcite cleavage segments ($4 \times 3 \times 1$ mm) were powdered and analyzed by powder X-ray diffraction (XRD) using a Phillips PW-1547 X-ray diffractometer (equipped with an automatic slit, with steps of 0.005°2θ and 4 s counting time), as well as Raman Spectrometry (HORIBA Jobin Yvon HR800 micro-Raman spectrometer using the 633 nm line of a He–Ne Laser) to detect any possible new phases formed on the calcite surface. The scattered Raman light was analyzed with a 100× objective in 180° backscatter geometry and a charged-coupled device (CCD) detector after being dispersed by a grating of 1800 grooves/mm. A confocal hole of 1000 μm, and a slit width of 100 μm were used, giving a resulting spectral resolution around 0.9 cm^{-1}. The longer term effect of phosphate solutions on calcite crystals with average sizes $2.5 \times 2.5 \times 0.8$ mm and calcite powders of ~7 mg (size fraction <10 μm) was studied by placing the calcite in Teflon vessels together with 50 mL of 50 mM $(NH_4)_2HPO_4$ solution and stirred continuously for 5 weeks. The powders were then filtered, rinsed with deionized water and dried and subsequently analyzed using XRD and scanning electron microscopy (SEM) (JEOL 6610-LV). The single crystals were also analyzed by XRD after crushing to a powder.

3. RESULTS

3.1. Effect of phosphate on etch pit shape and density

After flowing water over the $\{10\bar{1}4\}$ calcite surface, dissolution took place by the formation of characteristic rhombohedral shallow (one unit cell, ca. 3 Å) etch pits, limited by steps parallel to the $[\bar{4}41]_+$, $[48\bar{1}]_+$, $[\bar{4}41]_-$ and $[48\bar{1}]_-$ directions (Fig. 1). The subscripts (+ or −) follow the convention used by Paquette and Reeder (1995). These steps are bonded by alternating Ca^{2+} and CO_3^{2-} ions. Steps parallel to a given set of periodic bond chains (PBCs) are structurally non-equivalent (Liang et al., 1996; Liang and Baer, 1997). The structurally equivalent $[\bar{4}41]_-$ and $[48\bar{1}]_-$ steps are acute and intersect the bottom of the etch pit at an angle of 78°, while $[\bar{4}41]_+$ and $[48\bar{1}]_+$ steps are obtuse and intersect the bottom of the etch pit at an angle of 102° (Hay et al.,

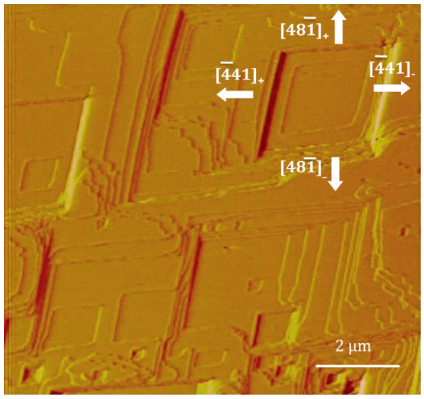

Fig. 1. AFM deflection image showing the development of shallow (one unit cell – 3.5 Å) rhombohedral etch pits during dissolution of the $\{10\bar{1}4\}$ calcite cleavage surface in deionized water (pH 6). The step retreat directions are indicated by arrows.

2003). Once formed the etch pits progressively retreat with increasing contact time with water. As a result, etch pits eventually merged with adjacent pits, effectively removing the entire unit cell layer. Occasionally, deeper etch pits formed.

AFM observations of calcite cleavage surfaces in the presence of all tested phosphate solutions resulted in dissolution of the calcite surfaces as seen in the development and continuous spreading of etch pits. However the presence of phosphate caused major changes in etch pit morphology and etch pit density compared to dissolution in deionized water. In all cases the shallow rhombohedral etch pits changed their morphology in the presence of phosphate-bearing solutions. Fig. 2a–c show a calcite surface after injection of 5 μM, 0.5 mM and 5 mM of $(NH_4)_2HPO_4$ solutions (pH ranging between 7.3 and 8.0) in the fluid cell, respectively. On contact with 5 μM phosphate solution no new etch pits were observed and instead rounding of preexisting steps was noticed. At $(NH_4)_2HPO_4$ concentrations between 0.1 and 0.5 mM etch pits nucleated showing step edges approximately parallel to the [0 1 0] direction, which gave them a pseudo-triangular appearance. As well, at this concentration significant increase in etch pit density per scanned area was observed (Fig. 3). Interestingly, on contact with 5 mM $(NH_4)_2HPO_4$ solution the etch pits again changed their appearance to a distorted rhombohedral form.

In the presence of Na_2HPO_4, (pH ~8) rounding of etch pits was already observed at 100 μM concentration. Progressive rounding with increasing phosphate concentration lead to the development of a new step edge parallel to the [0 1 0] direction, which resulted in a change in the morphology of the etch pits from rhombohedral to pseudo-triangular, as was observed in the presence of $(NH_4)_2HPO_4$ solutions. This change in morphology was evident from Na_2HPO_4 concentrations between 1 and 5 mM. However, a further increase in Na_2HPO_4 concentration above 50 mM resulted in a progressive elongation of the etch pits parallel to the $[42\bar{1}]$ direction, changing the appearance of the etch pits into heart shapes and tear shapes (Fig. 4a–c).

A similar evolution of etch pit morphology was observed in experiments with NaH_2PO_4 solutions (pH ranging from 4 to 5.5), shown in Fig. 5a–c. Slight rounding of etch pits was first detected at 500 μM, although it was more evident in the presence of a 10 mM NaH_2PO_4 solution, when pseudo-triangular etch pits were observed. Again, elongation of the etch pits parallel to $[42\bar{1}]$ direction was detected for NaH_2PO_4 concentrations above 50 mM (Fig. 5b). For these solutions, distorted rhombohedral morphologies were observed at concentrations above 0.5 M (Fig. 5c).

The etch pit morphology developed in the presence of $(NH_4)_2HPO_4$ with NaCl (0.1 M) to give a high ionic strength is presented in Fig. 5d–f. The etch pits showed rounded obtuse/obtuse corners at concentrations above 0.5 μM $(NH_4)_2HPO_4$ (Fig. 5d) and then returned to a slightly distorted rhombohedral form when a 1 M $(NH_4)_2HPO_4$ solution was passed over the calcite surface (Fig. 5e). This change in morphology was found to be reversible, and upon injection of a 0.5 μM $(NH_4)_2HPO_4$ solution into the fluid cell, the etch pits showed again rounded corners (Fig. 5f). In the presence of $MgCl_2$, curving of the etch pits was observed at the lowest phosphate concentration (0.5 μM), the etch pits changed their morphology to a triangular form already at a concentration of 100 μM and returned to a slightly distorted rhombohedral shape at 1 mM.

3.2. Effect of phosphate on calcite dissolution kinetics

The etch pit spreading rate in deionised water, calculated as summed spreading rates of obtuse $[\bar{4}41]_+$, $[48\bar{1}]_+$ and acute $[\bar{4}41]_-$, $[48\bar{1}]_-$ steps, was 1.9 (±0.45) nm/s, which is in agreement with values reported previously for dissolution of calcite under ambient conditions (e.g. Jordan and Rammensee, 1998; Ruiz-Agudo et al., 2010). Figs. 6 and 7 summarize the etch pit spreading rates measured and expressed as summed etch pit spreading rates. Dissolution in the presence of $(NH_4)_2HPO_4$ solutions (Fig 6a) (pH ranging from 5.6 to 8.1) resulted in inhibition of etch pit propagation for $(NH_4)_2HPO_4$ concentrations above 0.1 mM, when etch pit propagation rates decreased down to values around 0.7 nm/s (Fig. 6a). The spreading rate in the presence of Na_2HPO_4 (pH ~8) for all tested concentrations (Fig. 6b)

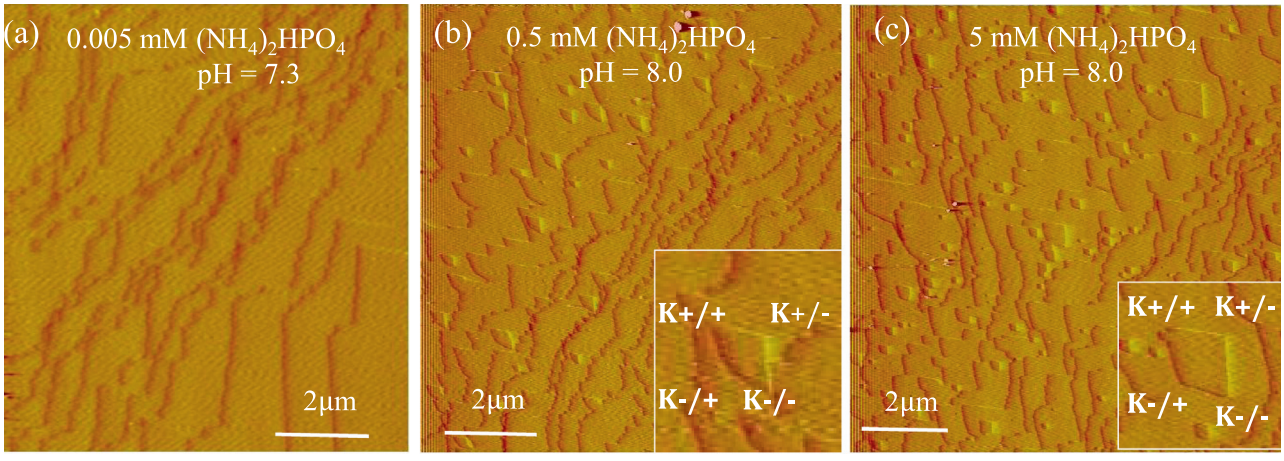

Fig. 2. AFM deflection images showing dissolution of calcite $\{10\bar{1}4\}$ cleavage surfaces in the presence of $(NH_4)_2HPO_4$ solutions. (a) Surface after injection of 5 μM; (b) after injection of 0.5 mM; (c) after injection of 5 mM.

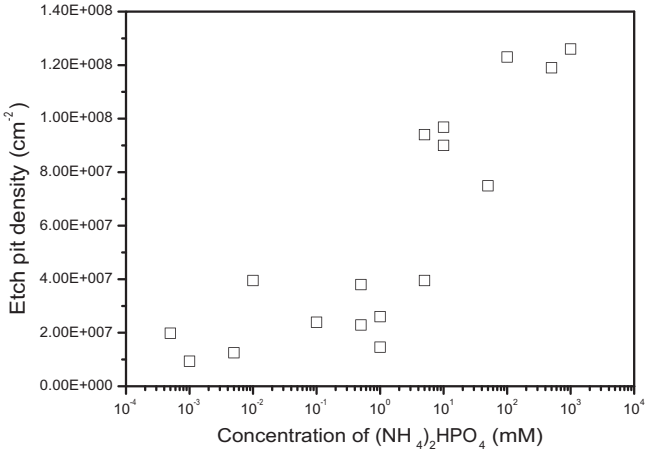

Fig. 3. Etch pit density (cm^{-2}) as a function of $(NH_4)_2HPO_4$ concentration.

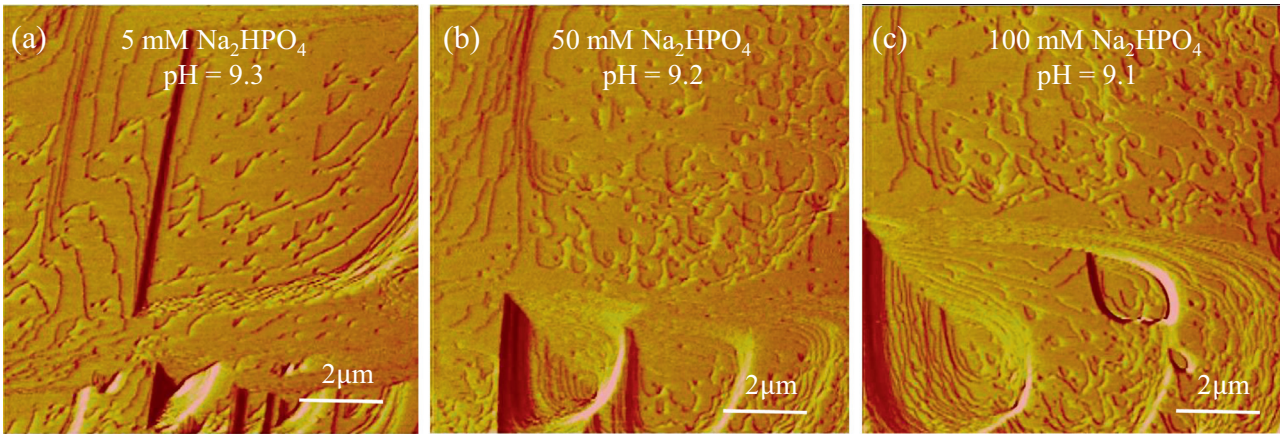

Fig. 4. AFM deflection images showing dissolution of calcite $\{10\bar{1}4\}$ cleavage surfaces in the presence of Na_2HPO_4 solutions. (a) Surface after injection of 5 mM; (b) after injection 50 mM; (c) and after injection of 100 mM. As a result, there is a rapid change in the density of etch pits and shapes at kink sites (K).

remained close to that measured in deionised water, and no significant trend was observed with increasing phosphate concentration (Fig. 6b). The etch pit spreading rate for NaH_2PO_4 solution having a lower pH (~4) was the highest rate compared to the other phosphate solutions tested. Etch pit propagation rate values are similar to those of deionised water up to 10 μM. For concentrations above 0.1 mM, dissolution rates increased significantly with respect to those measured in deionized water, reaching a maximum of 9.9 (±2.9) nm/s at 1 mM NaH_2PO_4 (Fig. 7a). Measurements of dissolution rates above 10 mM phosphate concentration were not possible due to the fast spreading and merging of etch pits and rapid removal of atomic layers.

The presence of NaCl and $MgCl_2$ to produce a higher ionic strength (IS) at a concentration of 0.1 M resulted in an increase in the etch pit spreading rate with respect to electrolyte-free $(NH_4)_2HPO_4$ solutions at the same phosphate concentration (Fig. 7b). The ionic strength of NaCl and $MgCl_2$ solutions 0.1 and 0.3, respectively, were calculated using the PHREEQC program (Parkhurst and Appelo, 1999). The average etch pit spreading rate in the presence of NaCl increased up to a maximum of 5.15 ± 0.82 nm/s at 1 mM $(NH_4)_2HPO_4$ and above this concentration started decreasing and eventually reached values similar to those measured in deionized water at a $(NH_4)_2HPO_4$ concentration of 100 mM. In the case of $MgCl_2$, only concentrations from 0.5 μM to 10 mM $(NH_4)_2HPO_4$ were tested because spontaneous precipitation occurred in the experimental solution at higher concentrations. Possibly, supersaturation with respect to a Mg-phosphate phase was reached during the experiments. The etch pit spreading rate values were close to those measured in deionised water (2.41 ± 0.36 nm/s) for $(NH_4)_2HPO_4$ concentrations ranging from 0.5 μM to 5 mM (Fig. 7b). Interestingly, the etch pit spreading rate significantly increased at 10 mM $(NH_4)_2HPO_4$ in the presence of $MgCl_2$ above the value measured in deionized water.

ICP-OES measurements revealed that the Ca_T concentration in the effluent solution did not significantly change with $(NH_4)_2HPO_4$ concentration, only showing a dramatic increase for concentrations above 100 mM (Fig. 8). Because these values were obtained during dissolution of the same

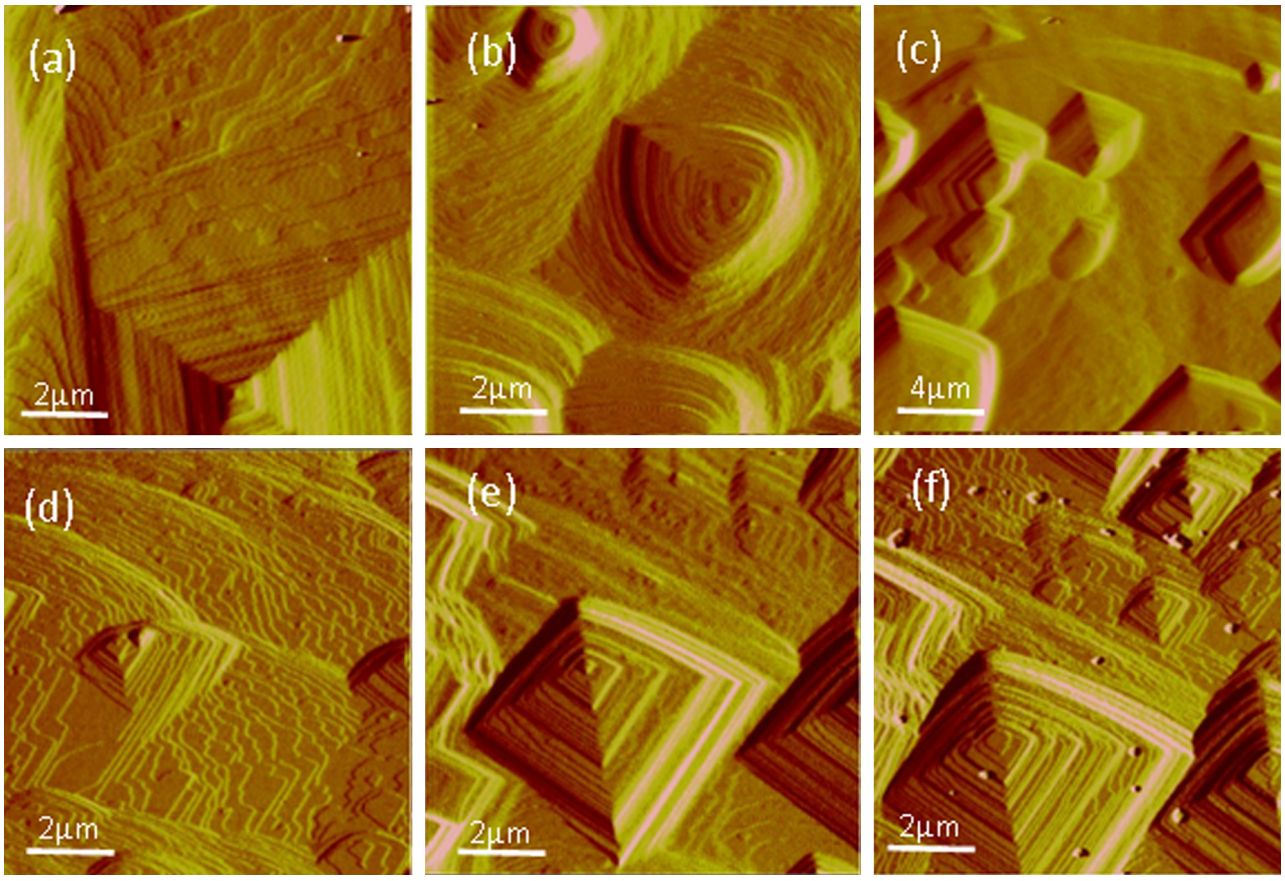

Fig. 5. AFM deflection images showing deep etch pits formed on the $\{10\bar{1}4\}$ calcite cleavage surface in the presence of NaH_2PO_4; (a) surface after injection of 500 µM; (b) after injection of 50 mM; (c) after injection of 100 mM. (d–f) Dissolution in the presence of $(NH_4)_2HPO_4$ + NaCl (0.1 M); (d) etch pits with rounded corner developed after injection of 500 mM phosphate solution; (e) recovery of (slightly distorted) rhombohedral form after injection of 1 M phosphate solution; (f) etch pits with rounded corner again after injection of 5 mM phosphate solution.

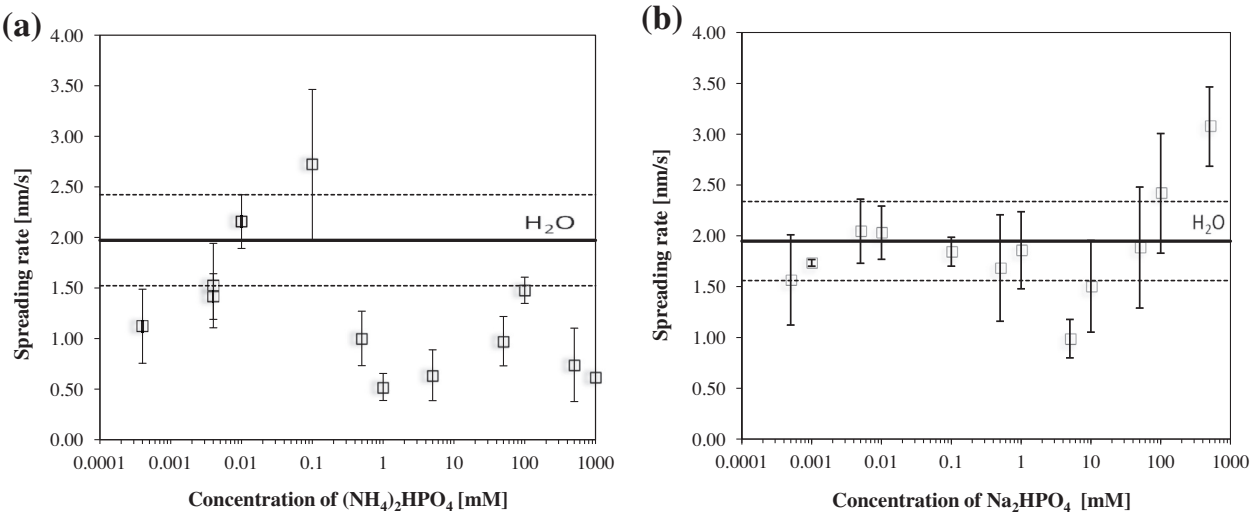

Fig. 6. Measured etch pit spreading rate (nm/s) as a function of (a) $(NH_4)_2HPO_4$ and (b) Na_2HPO_4 concentration (mM). The horizontal line and the dashed lines indicate the spreading rate range in deionized water.

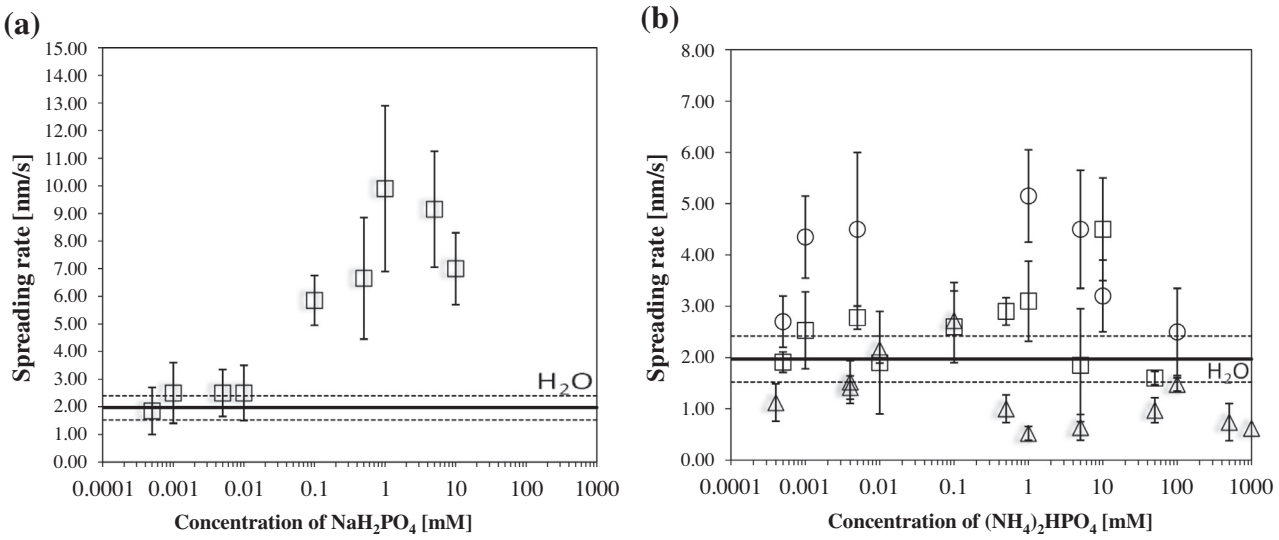

Fig. 7. Measured etch pit spreading rate (nm/s) as a function of (a) NaH_2PO_4 concentration (mM) and (b) concentration (mM) of $(NH_4)_2HPO_4$ (triangles), $(NH_4)_2HPO_4$ with 0.1 M NaCl (circles) and $(NH_4)_2HPO_4$ with 0.1 M $MgCl_2$ (squares). The horizontal line and the dashed lines indicate the spreading rate range in deionized water.

calcite fragment, they are reported as an indication of the trend followed by calcite dissolution rates with increasing phosphate concentration.

3.3. Simulation of the evolution of solution composition in the AFM fluid cell

The hypothetical batch reaction of calcite with various phosphate solutions was simulated using the speciation program PHREEQC (Parkhurst and Appelo, 1999). The final Ca^{2+} concentration in the fluid cell (solution volume 38 μL) once equilibrium was reached with respect to calcite (and assuming no precipitation of any Ca-P phases) is given in Table 1. The concentration of calcium calculated with PHREEQC increases continuously with increasing phosphate concentration. The calculated total concentration of

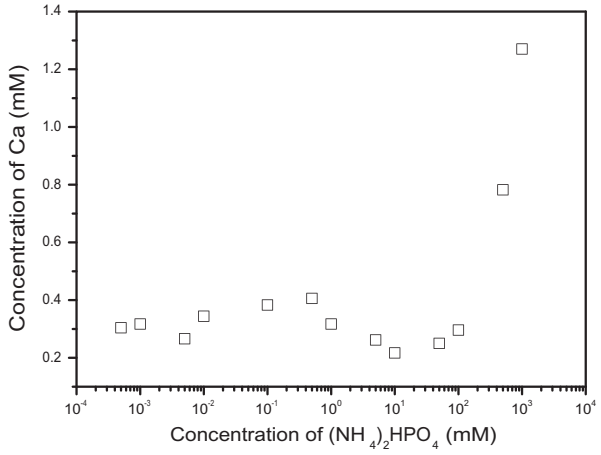

Fig. 8. [Ca^{2+}] (mM) determined by ICP-OES analysis of the effluent solutions from AFM dissolution experiments vs. concentration of $(NH_4)_2HPO_4$ (mM).

Ca^{2+} ions released during dissolution in $(NH_4)_2HPO_4$ (pH ~8) and NaH_2PO_4 (pH ~4) solutions was approximately one order of magnitude higher than in Na_2HPO_4 solutions for concentrations higher than 5 mM. The disagreement between the initial pH values measured and calculated using PHREEQC for solutions with low phosphate concentrations also given in Table 1 was most likely due to the low conductivity of ions for measurements in very dilute solutions. Table 2 presents the Saturation Indices (SI) of phosphate solutions with respect to the possible calcium phosphate phases upon equilibration with calcite, calculated using the phreeqc.dat database (Parkhurst and Appelo, 1999) and the solubility data presented by Wang and Nancollas (2008). In the case of solutions with higher ionic strength, that is, 0.1 M NaCl and 0.1 M $MgCl_2$ as background electrolytes and solutions with phosphate concentration >50 mM, saturation indexes were calculated using the wateq4f.dat database (Parkhurst and Appelo, 1999). Calculated SI values show that it could be thermodynamically possible for more than one calcium phosphate phase to precipitate if equilibrium were reached with respect to calcite. The two most likely Ca-phosphate phases are octacalcium phosphate ($Ca_8H_2(PO_4)_6{\cdot}5H_2O$, OCP) and hydroxyapatite ($Ca_5(PO_4)_3(OH)$, HAP), the former being more favorable because of its higher SI in all the experimental solutions. However, in our flow-through set up, equilibrium would not be reached and Ca^{2+} concentrations and SI are just used just as a reference for the maximum or threshold value in our experiments.

3.4. Precipitation of Ca-phosphate phases

The dissolution of calcite in the presence of phosphate solutions at pH ~8 (both $(NH_4)_2HPO_4$ and Na_2HPO_4) and NaH_2PO_4 (pH ~4.5) and concentrations higher than 5 mM resulted in precipitation of rounded nuclei on the dissolving calcite cleavage surface. Further, subsequent

Table 2
Saturation Indices (SI) for calcite and calcium phosphate phases (calculated using PHREEQC) in equilibrium with calcite.

Saturation Indices (SI)	0.0005	0.001	0.005	0.01	0.1	0.5	1	5	10	50(a)	100(a)	500(a)	1000(a)
	$(NH_4)_2HPO_4$ [mM]												
Calcite	0.00	0.00	0.00	0.00	0.00	0.01	0.00	0.00	0.00	0.00(0.00)	0.00(0.00)	0.00(0.00)	0.00(0.00)
Brushite	−4.04	−3.74	−3.03	−2.71	−1.48	2.90	−0.01	0.82	1.13	1.77(1.80)	2.04(2.09)	2.65(2.90)	2.94(3.35)
OCP	15.10	16.90	21.10	22.91	29.06	49.49	35.05	38.38	39.67	42.75(42.88)	44.19(44.49)	48.10(49.49)	50.33(52.35)
HAP	14.30	16.08	20.21	21.92	26.84	41.35	30.03	31.65	32.39	34.7(34.82)	36.00(36.28)	40.09(41.36)	42.78(44.36)
Monetite	−3.73	−3.43	−2.72	−2.40	−1.17	3.23	0.30	1.13	1.44	2.08(2.11)	2.35(2.40)	2.98(3.24)	3.29(3.70)
	Na_2HPO_4 [mM]												
Calcite	0.00	0.00	0.00	0.00	0.00	0.01	0.00	0.00	0.00	0.00(−1.18)	0.00(0.05)	0.11(0.00)	0.00(0.00)
Brushite	−4.04	−3.74	−3.04	−2.74	−1.74	−1.07	−0.81	−0.30	−0.11	0.32(0.34)	0.51(0.50)	1.07(1.04)	1.28(1.25)
OCP	15.10	16.90	21.07	22.86	28.51	31.78	32.91	35.07	35.86	37.62(36.10)	38.43(38.36)	41.20(41.08)	42.21(42.31)
HAP	14.30	16.09	20.25	22.01	27.30	29.82	30.54	31.79	32.23	33.17(29.99)	33.64(33.51)	35.79(35.74)	36.48(36.88)
Monetite	−3.74	−3.43	−2.74	−2.43	−1.43	−0.76	−0.50	0.01	0.20	0.63(0.67)	0.82(0.82)	1.40(1.36)	1.63(1.60)
	NaH_2PO_4 [mM]												
Calcite	0.00	0.00	0.00	0.00	0.00	−0.01	0.00	0.01	−0.02	0.00(0.00)	0.00(0.20)	0.00(0.00)	0.00(0.00)
Brushite	−4.04	−3.74	−3.03	−2.72	−1.52	−0.38	0.89	0.89	1.15	1.68(1.80)	1.88(1.90)	2.29(2.34)	2.46(3.35)
OCP	15.09	16.90	21.09	22.88	28.83	32.84	36.44	36.44	37.12	38.78(42.88)	39.36(39.52)	40.54(40.93)	40.99(52.35)
HAP	14.29	16.08	20.21	21.93	26.63	27.78	27.37	27.37	27.17	27.29(34.82)	27.27(27.49)	27.11(27.63)	26.99(44.36)
Monetite	−3.73	−3.43	−2.72	−2.41	−1.21	−0.07	0.39	1.20	1.46	1.99(2.11)	2.19(2.21)	2.62(2.66)	2.80(3.70)

(a) Values in brackets calculated using Wateq4f database.
OCP-octacalcium phosphate-log $K_{sp} = 96.6$ (Wang and Nancollas, 2008).
HAP-hydroxylapatite-log $K_{sp} = 116.8$ (Wang and Nancollas, 2008).

growth in height and length of these initial nuclei, oriented parallel to the [42$\bar{1}$] direction occurred. At these solution concentrations, growth was observed immediately on the calcite surface on contact with the phosphate solutions at concentrations >5 mM (Fig. 9a). The growth particles eventually merged and formed a monolayer (approximately 4 nm high) (Fig. 9b). At concentrations higher than 50 mM, when dissolution of the calcite substrate was faster, growth in length was less pronounced but the height of the particles continued to increase up to 10 nm, while the calcite surface below was simultaneously dissolving (Fig. 9c). Moreover, after approximately 1 h of continuous flow of a 50 mM $(NH_4)_2HPO_4$ solution, the particles nucleated at calcite surface steps developed crystallographic faces mostly orientated along the [010] direction (Fig. 8d).

After exposure of several calcite surfaces to phosphate-containing solutions, the calcite crystals were removed from the AFM fluid cell and analyzed using Raman spectroscopy and XRD. Results of the Raman analysis are presented in Fig. 10. Analysis of the band assignments showed Raman active bands for calcite at 284, 715 and 1087 cm^{-1} (Gunasekaran et al., 2006). The band located at 284 cm^{-1} represents translational lattice mode T($CaCO_3$) vibrations, whereas bands at 715 and 1087 cm^{-1} are responsible for symmetric CO_3 deformation and symmetric η_4CO_3 stretching vibrations. Additional bands were observed at 430 and at 961 cm^{-1}. The band at 961 cm^{-1} corresponds to the ν_1PO_4 mode of P-O vibrations in apatite, but both bands (430 and 961 cm^{-1}) are also characteristic of carbonated Ca-P phases (Crane et al. 2006; Wang et al., 2012a,b). The determined FWHM (full width at half maximum) of 15 cm^{-1} of the ν_1PO_4 band is relatively high, indicating the formation of a slightly disordered carbonated apatite on the surface of the calcite. No additional phosphate bands characteristic for transient calcium phosphate phases were observed. X-Ray diffraction analysis of calcite single crystals from AFM experiments after contact with phosphate solutions showed no additional peaks different to those corresponding to calcite. However, the XRD pattern of calcite powder after long-term contact (5 weeks) with a 50 mM $(NH_4)_2HPO_4$ solution showed the presence of an additional mineral phase, identified as hydroxyapatite (See Supplementary material).

4. DISCUSSION

4.1. Effect of phosphate on the morphology of dissolution features

The results presented here show a significant effect of phosphate on the morphology of etch pits developed on calcite surfaces during dissolution. The characteristic

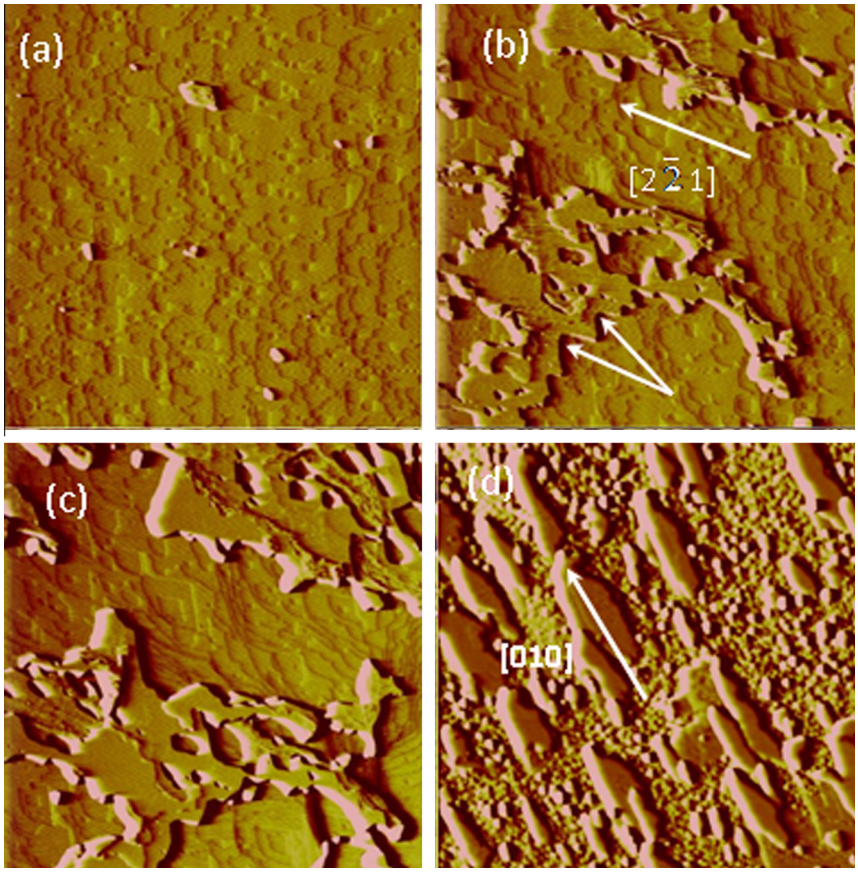

Fig. 9. AFM deflection images showing the growth of a Ca-phase on the simultaneously dissolving calcite surface: (a) initial particles forming; (b) two dimensional nucleation on the surface along [2$\bar{2}$1] step and step edges forming - indicated by arrows; (c) monolayer forming on the dissolving surface; (d) crystals with crystallographic faces forming along the edge [010] of the step. All images 10 × 10 μm.

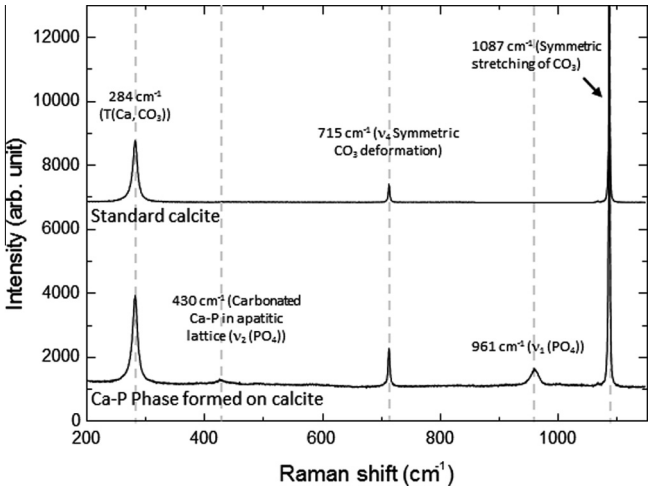

Fig. 10. Raman spectra of a calcite surface after exposure to phosphate-containing solutions in the AFM fluid cell. Vibration bands were assigned for calcite and a Ca-P phase.

rhombohedral shape showed a rounding of +/+ etch pit corners, changing to pseudo-triangular forms with increasing phosphate concentration and finally to tear shapes and/or distorted rhombohedra. The fact that similar morphological effects are observed in both sodium and ammonium phosphate solutions suggest that these changes are due to the presence of phosphate. Changes in etch pit morphology in the presence of phosphate-bearing solutions have previously been reported (Wang et al., 2012a,b). Other researchers have also documented etch pit modifications from observations made during calcite dissolution in the presence of different inorganic species. Vavouraki et al. (2010) and Ruiz-Agudo et al. (2010) observed a change in etch pit shape from the typical rhombohedral morphology to a pseudo-hexagonal form during calcite dissolution in solutions containing F^- ions. Pérez-Garrido et al. (2007) observed similar effects during dissolution in the presence of Cd^{2+} ions. Ruiz-Agudo et al. (2010) reported changes in etch pit morphology when Li^+ was present in solution during the dissolution of calcite, very similar to those observed here in the presence of phosphate.

The change from the usual rhombohedral morphology observed during calcite dissolution and growth in pure solutions is frequently ascribed to the pinning or adsorption of foreign ions at specific surface sites (for a comprehensive review see Ruiz-Agudo and Putnis, 2012). Phosphate adsorption on calcite was investigated by De Kanel and Morse (1978) in comparison with aragonite, showing that although aragonite adsorbs much more phosphate than calcite in the initial stages of the process, the uptake rate for calcite decreases more slowly than that for aragonite. This suggests that calcite could be an important sink for phosphate in marine sedimentary environments. Phosphate adsorption during calcite growth is considered to follow a step pinning model (Dove and Hochella, 1993). Berner and Morse (1974) describe in detail that process and state that if the lateral distance between the two inhibitor ions (pinned sites) is smaller than the diameter of the critical hole, then the curvature increases and the holes are likely to be filled back and no step advancement can be observed. Otherwise, when the lateral distance between inhibitor ions is larger than the critical hole, then the advancement of the step can continue, causing a decrease in the curvature of the step (see Lasaga and Luttge, 2001, for further clarification). This process could to some extent explain the curving of +/+ corners observed for low phosphate concentrations. Nevertheless, it has been recently shown that morphological changes observed in growth and dissolution features, when some foreign ions (i.e. different to those building the crystal) are present in solution, may also be explained in terms of the changes in the hydration of the mineral surface induced by the background ions (Kowacz and Putnis, 2008; Ruiz-Agudo et al., 2010; Kowacz et al., 2010; Wang et al., 2012a,b). In terms of this model, the evolution in etch pit morphology observed in this study could be explained as the result of progressive stabilization of polar faces (those with a net dipole moment), which are not stable under normal (i.e. pure solutions) growth and dissolution conditions (see Fig. 11). The presence of background ions tends to stabilize water molecules in ion hydration shells and at the crystal surface. Increasing ion hydration reduces both repulsive interactions between ions of the same charge and attractive interactions between ions of opposite charges. Thus, polar faces will be stabilized while non-polar faces should be less stable in electrolyte solutions. Stabilization of (0001) faces by phosphate ions during calcite dissolution is consistent with the development of a new step edge parallel to [010] since the direction of the new edge corresponds to the intersection of the {0001} form with the cleaved rhombohedron $\{10\bar{1}4\}$, this leading first to the rounded appearance of the etch pits and subsequently to the pseudo-triangular form (Fig. 11b and c). {0001} faces consist of alternate layers of Ca^{2+} and CO_3^{2-} ions in successive planes, thus having a net dipole moment. The subsequent evolution of the etch pit morphology (i.e. from triangular to tear-shape and/or distorted rhombohedra) can also be interpreted in the same terms (Fig. 11d and e). Such morphologies could develop as a result of the elongation of etch pits along the $[42\bar{1}]$ direction. Again, this direction is not stable under normal growth conditions

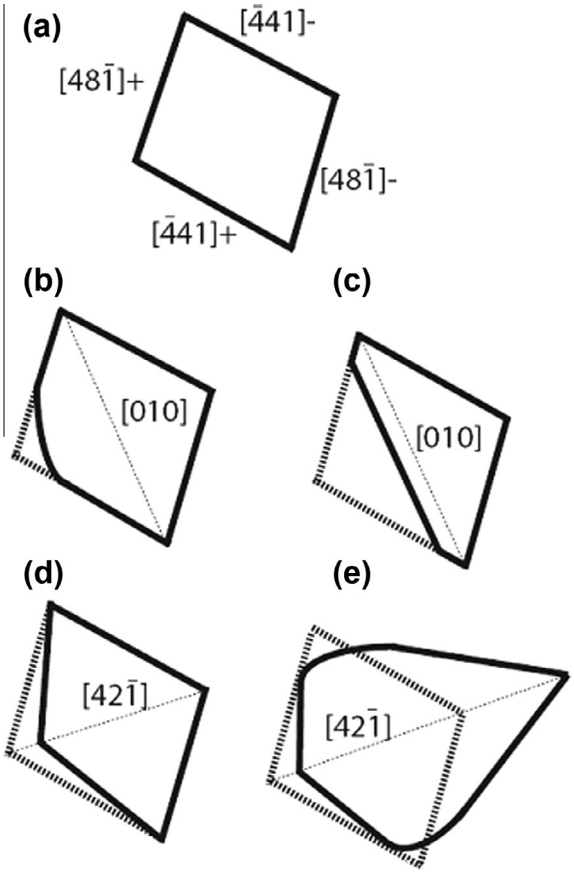

Fig. 11. Schematic representation of etch pit shape evolution showing (a) typical rhombohedral etch pits formed upon contact of calcite cleavage surfaces with deionized water and changes in etch pit morphology induced by the presence of phosphate ions: (b) rounding of +/+ etch pit corners, (c) pseudo-triangular forms, (d) distorted rhombohedra and (e) tear shapes.

due to its polar character, but becomes increasingly stable due to the presence of phosphate ions. Changes in the morphology of dissolution features developed on gypsum surfaces in the presence of phosphate ions have also been reported (Pinto et al. 2010). Stabilization of polar steps (parallel to the [1 0 1] direction) by phosphate ions has been suggested to explain such observations.

4.2. Effect of phosphate on etch pit spreading rate and density

Our experiments show no significant effect of phosphate on the spreading rate of etch pits in the presence of Na_2HPO_4 (pH ~8.0) for all the concentration tested and in the presence of NaH_2PO_4 solutions up to ca. 0.05 mM (pH ~5.5). Inhibition of the etch pit spreading rate was observed however, in the presence of $(NH_4)_2HPO_4$ in the range of concentration tested (pH between 5.6 and 8.1). This leads us to hypothesize that this inhibitory effect observed could be due to the presence of NH_4^+, and not to the presence of phosphate, as inhibition was not observed for the Na-phosphate-salts for the same range of pH. Moreover, the results reported by Dove and Hochella (1993) regarding the inhibitory effect of phosphate on calcite growth could have a similar origin, as NH_4^+ was also present in their growth solutions. Morse (1974) showed, in agreement with our observations, that phosphate inhibits calcite dissolution, this effect being also dependent on the degree of saturation of the solution. Unfortunately, the phosphate salt used in their experiments is not indicated in this paper nor in others by the same authors reporting similar results (e.g. Berner and Morse, 1974). The propagation rate of etch pits formed upon calcite dissolution is virtually pH-independent for pH values above ca. 5.5–6.0 (Wang et al., 2012a,b). However, it is significantly accelerated with decreasing pH below this value. Thus, the increase in etch pit propagation rate (with respect to deionized water) observed for NaH_2PO_4 concentrations higher than 0.1 mM could be simply due to the lower pH of these solutions (see Table 1). Alkattan et al. (2002) studied the dissolution of a calcite disc in the presence of sodium polyphosphate solution in highly acidic conditions ($-1 < pH < 3$). Their results showed that phosphate inhibits its dissolution at these highly acidic conditions, but the ability of phosphate to inhibit calcite dissolution decreases with increasing pH for $pH > 1$.

Additionally, increasing phosphate concentration resulted in a large increase in etch pit density up to a maximum value of $\sim 1.3 \times 10^8\ cm^{-2}$. This suggests that the PO_4 species is involved. Values of etch pit density higher than defect density have been related to nucleation of pits on defect-free surfaces under far from equilibrium conditions (which is the case for our solutions) as well as to the presence of specific ionic species in solution (see Ruiz-Agudo and Putnis, 2012 and references therein). Ruiz-Agudo et al. (2009) have shown the increased etch pit density during the dissolution of calcite in the presence of Mg^{2+}. An explanation given there is the ability of Mg^{2+} to disrupt the hydration environment of the calcite surface and hence to reduce the energy barrier needed for unassisted etch pit nucleation. In a similar way it is suggested that PO_4 also either alters the hydration environment at the calcite surface or directly adsorbs at the surface. Whatever the mechanism, the energy barrier for etch pit formation must be reduced to result in the high etch pit density.

Overall dissolution rates (inferred here from the calcium concentration measured in the AFM outflow) and etch pit propagation rates reflect similar effects of phosphate concentration on the kinetics of calcite dissolution for phosphate concentrations $\leqslant$100 mM.

However, while overall dissolution rates will be affected by the precipitation of a secondary phase, etch pit spreading rate measurements will not reflect the influence of this process. Thus, we believe that direct comparison of these parameters is not relevant in this case.

The calcium concentration in the outlet solution may be buffered by the precipitation of the secondary Ca-P phase. However, at high phosphate concentration, the observed rise in etch pit density that would significantly enhance the rate of calcium release to the solution, could explain the significant increase in the measured calcium concentration in the effluent solution. The possibility cannot be fully ruled out that this observation is related to the increase in

roughness (and thus, in the reactive surface area) upon progressive dissolution of the calcite crystal. Nevertheless, this seems highly unlikely as we observed directly that calcite dissolution occurred mostly as a layer-by-layer process, where new etch pits were created upon removal of complete atomic layers, without significant deepening of the etch pits.

4.3. The growth of Ca-phosphate phases on calcite surfaces

In our experiments, nucleation and growth of a Ca-P phase occurred on flat terraces containing actively dissolving etch pits on the calcite surface and to a lesser extent on steps. Precipitation was detected at phosphate concentrations >5 mM (pH ~8), although most nucleation and growth was observed at 50 mM. At these phosphate concentrations the dissolution of the calcite substrate released sufficient Ca^{2+} ions for the nucleation of the new Ca-P phase, which has been identified by Raman and XRD as a carbonate-containing hydroxyapatite. Thus the growth of the new phase was limited by the dissolution of calcite, coupled with the nucleation of the new phase. In all experiments, the phosphate solution flowing over the calcite surface was initially undersaturated with respect to any possible precipitating phase. If the initial amount of calcite dissolved and mixed with the bulk solution, thermodynamic calculations indicate that the solution would be supersaturated with respect to various Ca-P phases, as shown in Table 2. However, as stated above, in our flow-through experimental set up, equilibrium would not be reached (due to the continuous flow of solution) and this state is just a reference for the maximum or threshold supersaturation that could be reached theoretically in our experiments.

In any case, our observations indicate that, as a result of some initial dissolution of the calcite, the fluid in contact with the calcite interface must have been immediately supersaturated with respect to a Ca-P phase that precipitated. In our experiments, the growth of the Ca-P phase occurred initially by the attachment of nuclei seemingly randomly over the calcite surface. Some of the nuclei dissolved at the beginning of the growth period, to be replaced by further growth elsewhere. As well, preferential sites for growth were observed (indicated by arrows on Fig. 9b) along etch pit edges and at nucleation sites already established. With time, the main growth direction developed along one preferred direction $[4\,2\,\bar{1}]$.

The observation of a reaction product on a calcite surface exposed to diammonium hydrogenphosphate solutions has been previously recorded by AFM (Kamiya et al., 2004). The results of that preliminary study showed that the amount of reaction products increased with immersion time and increasing concentration of diammonium hydrogenphosphate. However our results more precisely determine the dissolution conditions for the growth of the new phase. Wang et al. (2012a,b) also used AFM to record the direct imaging of nano-clusters of Ca-phosphate on a calcite surface. Several other recent AFM studies have shown *in situ* the growth of new phases on a dissolving mineral surface. Heteroepitaxial growth of brushite ($CaHPO_4 \cdot 2H_2O$) on gypsum ($CaSO_4 \cdot 2H_2O$) cleavage surfaces was studied using *in situ* AFM by Pinto et al. (2010), who observed nucleation and growth of brushite crystals after contact of gypsum surfaces with phosphate bearing solutions, that were initially undersaturated with respect to any Ca-P phase. The growth of brushite crystals was mainly observed in areas of fast dissolution of gypsum, such as along higher step edges. Urosevic et al. (2012) observed the growth of a Mg-carbonate phase during simultaneous dissolution of dolomite ($CaMg(CO_3)_2$) in acidic solutions. As well, Ruiz-Agudo et al. (2012) have also recently reported the mechanism of leached layer formation during chemical weathering of silicate minerals, giving the example of wollastonite ($CaSiO_3$) dissolution in *in situ* AFM experiments. In this case precipitation was also observed simultaneously with congruent dissolution. In both dolomite and wollastonite dissolution experiments the bulk solution was undersaturated with respect to any possible precipitating phase. These latter two examples are interesting in also showing that direct observations combined with compositional analysis of reaction fluids as well as mineral precipitates, give clear evidence that a new phase is formed in a two step process: (1) stoichiometric dissolution of the mineral surface and; (2) subsequent precipitation of a secondary phase from a supersaturated fluid boundary layer in contact with the mineral surface. Such a mechanism differs from the well accepted model of preferential leaching of cations aimed at explaining non-stoichiometric release ratios (i.e., the elemental molar ratios measured in the fluid are different to those in the solid, especially at the initial stages of dissolution) observed during dolomite dissolution experiments (e.g. Busenberg and Plummer, 1982). Carbonation processes probably occur by the same mechanism (Daval et al., 2009; Hövelmann et al., 2012). Most recently Hellmann et al. (2003, 2012) have also suggested that the weathering of silicate minerals proceeds by interfacial dissolution of the parent mineral and precipitation of amorphous hydrated silica, forming a surface layer, which has a sharp chemical compositional change with the original mineral.

4.4. The influence of high ionic strength on calcite dissolution in the presence of phosphate solutions

Effects of background electrolytes on crystal dissolution and growth has been recently studied by Kowacz and Putnis (2008) and Ruiz-Agudo et al. (2010, 2011), and they suggested that the ability of background ions to modify solvent structure and ion hydration could explain the observed specific effects on dissolution and growth rates.

In our experiments the dissolution of calcite in the presence of phosphate at high ionic strength (IS), resulted in higher calcite dissolution rates in comparison to $(NH_4)_2HPO_4$ without added salts (lower IS). This could be attributed mostly to changes in solubility. The strong long-range electric fields emanating from the background ions reduce the activity of the building units of the crystal due to charge screening, hence increasing its solubility. Thus, considering purely thermodynamic effects, mineral dissolution rates at high ionic strength should increase due to the decreased free energy of the system. However, despite the similar high ionic strength of the solutions having $MgCl_2$ compared to those with NaCl, dissolution rates were systematically lower in

the presence of the former. This suggests some kind of specific effect of Mg^{2+} on calcite dissolution, which results in decreased etch pit spreading rates compared to those measured in the presence of Na (and high IS). This is in agreement with the results shown by Ruiz-Agudo et al. (2009), who reported inhibition of etch pit spreading rates on calcite cleavage surfaces by Mg^{2+}. This is attributed to element specific surface reactions possibly resulting from the blocking of etch pit spreading due to the incorporation of magnesium as $MgCO_3^0$ at kink/step sites in +/+ corners, possibly through surface reaction with $>CaOH_2^+$ sites. Alternatively Mg^{2+} is a more highly hydrated ion and therefore induces different solution hydration effects at the mineral–water interface.

5. CONCLUDING REMARKS AND IMPLICATIONS

Although the inhibitory effect of $(NH_4)_2HPO_4$ solutions on calcite dissolution has been confirmed, Na-phosphate solutions do not significantly inhibit dissolution. This tends to indicate that NH_4^+ may have a role to play in the inhibition process.

The direct observations of the AFM experiments described here show that during the interaction of calcite surfaces with phosphate-bearing solutions at slightly acidic to slightly alkaline pHs, the dissolution of a calcite substrate is coupled with the precipitation of a Ca-phosphate phase. The mechanism of interface-coupled dissolution-precipitation has been suggested as the controlling mechanism in many Earth processes (Putnis, 2002, 2009; Putnis and Putnis, 2007). The sequestration of phosphorus from solutions in contact with calcium carbonate minerals is therefore another example of this mechanism in practice. The implications of these observations are that calcium carbonate could effectively remove phosphorus from contaminated waters.

ACKNOWLEDGEMENTS

This work was carried out within the EU Initial Training Network (ITN) Delta-Min (Mechanisms of Mineral Replacement Reactions) grant PITN-GA-2008-215360. Jolanta Klasa acknowledges the receipt of a ESR (early stage research position) within this ITN. E. Ruiz-Agudo also acknowledges the receipt of a postdoctoral position in Delta-Min as well as a Ramón y Cajal grant from Spanish Ministery of Economy and Competitivy and funding from the project P11-RNM-7550 (Junta de Andalucía) and the project MAT2012-37584 (Ministery of Economy and Competitivy). L.J. Wang thanks the National Natural Science Foundation of China for a grant support (No. 41071208). Experimental facilities in Münster are supported by the DFG (German Research Foundation). The authors thank Veronika Rapelius and Angelika Breit (University of Münster) for help with ICP-OES and XRD analyses. We are grateful to three anonymous referees and Dr. Wogelius for their careful reviews and constructive comments that helped us to improve the quality of this manuscript.

APPENDIX A. SUPPLEMENTARY DATA

Supplementary data associated with this article can be found, in the online version, at http://dx.doi.org/10.1016/j.gca.2013.03.025.

REFERENCES

Alkattan M., Oelkers E. H., Dandurand J.-L. and Schott J. (2002) An experimental study of calcite dissolution rates at acidic conditions and 25 °C in the presence of $NaPO_3$ and $MgCl_2$. *Chem. Geol.* **190**, 291–302.

Berner R. A. and Morse J. W. (1974) Dissolution kinetics of calcium carbonate in sea water IV. Theory of calcite dissolution. *Am. J. Sci.* **274**, 108–134.

Busenberg E. and Plummer L. (1982) The kinetics of dissolution of dolomite in CO_2 H_2O systems at 1.5 to 65 degrees C and 0 to 1 atm pCO_2. *Am. J. Sci.* **282**, 45–78.

Crane N. J., Popescu V., Morris M. D., Steenhuis P. and Ignel M. A. (2006) Raman spectroscopic evidence for octacalcium phosphate and species deposited during intramembranous mineralisation. *Bone* **39**, 434–442.

Daval D., Martinez I., Guigner J.-M., Hellmann R., Corvisier J., Findling N., Dominici C., Goffé B. and Guyot F. (2009) Mechanism of wollastonite carbonation deduced from micro- to nanometer length scale observations. *Am. Mineral.* **94**, 1707–1726.

De Kanel J. and Morse J. W. (1978) The chemistry of orthophosphate uptake from seawater on to calcite to aragonite. *Geochim. Cosmochim. Acta* **42**, 1335–1340.

Dove P. M. and Hochella M. F. J. R. (1993) Calcite precipitation mechanisms and inhibition by orthophosphate: *in situ* observations by Scanning Force Microscopy. *Geochim. Cosmochim. Acta* **57**, 705–714.

Elser J. and Bennett E. (2011) A broken biogeochemical cycle. *Nature* **478**, 29–31.

Gunasekaran S., Anbalagan G. and Pandi S. (2006) Raman and infrared spectra of carbonates of calcite structure. *J. Raman Spectrosc.* **37**, 892–899.

Hay M. B., Workman R. K. and Manne S. (2003) Mechanisms of metal ion sorption on calcite: composition mapping by lateral force microscopy. *Langmuir* **19**, 3727–3740.

Hellmann R., Penisson J. M., Hervig R. L., Thomassin J. H. and Abrioux M. F. (2003) An EFTEM/HRTEM high-resolution study of the near surface of labradorite feldspar altered at acid pH: evidence for interfacial dissolution-reprecipitation. *Phys. Chem. Miner.* **30**, 192–197.

Hellmann R., Wirth R., Daval D., Barnes J.-P., Penisson J.-M., Tisserand D., Epicier T., Florin B. and Hervig R. L. (2012) Unifying natural and laboratory chemical weathering with interfacial dissolution-reprecipitation: a study based on the nanometer-scale chemistry of fluid-silicate interfaces. *Chem. Geol.* **294–295**, 203–216.

Hövelmann J., Putnis C. V., Ruiz-Agudo E. and Austrheim H. (2012) Direct nanoscale observations of CO_2 sequestration during brucite $[Mg(OH)_2]$ dissolution. *Environ. Sci. Technol.* **46**, 5253–5260.

Jacobs J. J., Gilbert J. L. and Urban R. M. (1998) Current concepts review – corrosion of metal orthopaedic implants. *J. Bone Joint Surg. (Am.)* **80**, 268–282.

Jamtveit B. and Austrheim H. (2010) Metamorphism: the role of fluids. *Elements* **6**, 156–158.

Jordan G. and Rammensee W. (1998) Dissolution rates of calcite $(10\bar{1}4)$ obtained by scanning microtopography-based dissolution kinetics on surfaces with anisotropic step velocities. *Geochim. Cosmochim. Acta* **62**, 941–947.

Kamiya M., Hatta J., Shimada E., Ikuma Y., Yoshimura M. and Monma H. (2004) AFM analysis of initial stage of reaction between calcite and phosphate. *Mater. Sci. Eng. B* **111**, 226–231.

Karageorgiou K., Paschalis M. and Anastassakis G. N. (2007) Removal of phosphate species from solution by adsorbtion

onto calcite used as natural adsorbent. *J. Hazard. Mater.* **A139**, 447–452.

Kowacz M. and Putnis A. (2008) The effect of specific background electrolytes on water structure and solute hydration: consequences for crystal dissolution and growth. *Geochim. Cosmochim. Acta* **72**, 4476–4487.

Kowacz M., Prieto M. and Putnis A. (2010) Kinetics of crystal nucleation in ionic solutions: electrostatics and hydration forces. *Geochim. Cosmochim. Acta* **74**, 469–481.

Lea A. S., Amonette J. E., Baer D. R., Liang Y. and Colton N. G. (2001) Microscopic effects of carbonate, manganese, and strontium ions on calcite dissolution. *Geochim. Cosmochim. Acta* **65**, 369–379.

Lee M. R., Brown D. J., Hodson M. E., MacKenzie M. and Smith C. L. (2008) Weathering microenvironments on feldspar surfaces: implications for understanding fluid-mineral reactions in soils. *Mineral. Mag.* **72**, 1319–1328.

Liang Y. and Baer D. R. (1997) Anisotropic dissolution at the $CaCO_3$ $(10\bar{1}4)$ water interface. *Surf. Sci.* **373**, 275–287.

Liang Y., Baer D. R., McCoy J. M. and LaFemina J. P. (1996) Interplay between step velocity and morphology during the dissolution of $CaCO_3$ surface. *J. Vac. Sci. Technol. A* **14**, 1368–1375.

Lasaga A. C. and Luttge A. (2001) Variation of crystal dissolution rate based on a dissolution stepwave model. *Science* **291**, 2400–2404.

Morse J. W. (1974) Dissolution kinetics of calcium carbonate in sea water. V. Effects of natural inhibitors and position of the chemical lysocline. *Am. J. Sci.* **274**, 638–647.

Morse J. W. and Arvidson R. S. (2002) The dissolution kinetics of major sedimentary carbonate minerals. *Earth-Sci. Rev.* **58**, 51–84.

Paquette J. and Reeder R. J. (1995) Relationship between surface structure, growth mechanism and trace element incorporation in calcite. *Geochim. Cosmochim. Acta* **59**, 735–7499.

Parkhurst D. L. and Appelo C. A. J. (1999) Users guide to PHREEQC (version 2) – a computer program for speciation, batch reaction, one dimensional transport, and inverse geochemical calculations. *U.S. Geological Survey Water-Resources Investigation Report* **99-4259**, 312pp.

Pérez-Garrido C., Fernández-Díaz L., Pina C. M. and Prieto M. (2007) In situ AFM observations of the interaction between calcite $(10\bar{1}4)$ surfaces and Cd-bearing aqueous solutions. *Surf. Sci.* **601**, 5499–5509.

Pinto A. J., Ruiz-Agudo E., Putnis C. V. and Putnis A. (2010) AFM study of the epitaxial growth of brushite ($CaHPO_4{\cdot}2H_2O$) on gypsum cleavage surfaces. *Am. Mineral.* **95**, 1747–1757.

Putnis A. (2002) Mineral replacement reactions: from macroscopic observations to microscopic mechanisms. *Mineral. Mag.* **66**, 689–708.

Putnis A. (2009) Mineral replacement reactions. In *Reviews in Mineralogy and Geochemistry* (eds. E. H. Oelkers and J. Schott) MSA 70. pp. 87–124.

Putnis A. and Austrheim H. (2010) Fluid induced processes: metasomatism and metamorphism. *Geofluids* **10**, 254–269.

Putnis A. and John T. (2010) Replacement processes in the Earth's crust. *Elements* **6**, 159–164.

Putnis A. and Putnis C. V. (2007) The mechanism of reequilibration of solids in the presence of a fluid phase. *J. Solid State Chem.* **180**, 1783–1786.

Putnis C. V., Kowacz M. and Putnis A. (2008) The mechanism and kinetics of DTPA-promoted dissolution of barite. *Appl. Geochem.* **23**, 2778–2788.

Ren G., Reddy V. S., Cheng A., Melnyk P. and Mitra A. K. (2001) Visualisation of water-selective pore by electron crystallography in vitreous ice. *Proc. Natl. Acad. Sci. U.S.A.* **98**, 1398–1403.

Ruiz-Agudo E. and Putnis C. V. (2012) Direct observations of mineral–fluid reactions using Atomic Force Microscopy: the specific example of calcite. *Mineral. Mag.* **76**, 227–253.

Ruiz-Agudo E., Putnis C. V., Rodriguez-Navarro C. and Putnis A. (2012) The mechanism of leached layer formation during chemical weathering of silicate minerals. *Geology.* **40**, 947–950.

Ruiz-Agudo E., Mees F., Jacobs P. and Rodriguez-Navarro C. (2007) The role of saline solution properties on porous limestone salt weathering by magnesium and sodium sulfates. *Environ. Geol.* **52**, 269–281.

Ruiz-Agudo E., Putnis C. V., Lopez-Jimenez C. and Navarro-Rodriguez C. (2009) An atomic force microscopy study of calcite dissolution in saline solutions: the role of magnesium ions. *Geochim. Cosmochim. Acta* **73**, 3201–3217.

Ruiz-Agudo E., Kowacz M., Putnis C. V. and Putnis A. (2010) The role of background electrolytes on the kinetics and mechanism of calcite dissolution. *Geochim. Cosmochim. Acta* **74**, 1256–1267.

Ruiz-Agudo E., Putnis C. V., Wang L. and Putnis A. (2011) Specific effects of background electrolytes on the kinetics of step propagation during calcite growth. *Geochim. Cosmochim. Acta* **75**, 3803–3814.

Schachtmann D. P., Reid R. J. and Ayling S. M. (1998) Phosphorous uptake by plants: from soil to cell. *Plant Physiol.* **116**, 447–453.

Sø H. U., Postma D., Jakobsen R. and Larsen F. (2011) Sorption of phosphate onto calcite; results from batch experiments and surface complexation modelling. *Geochim. Cosmochim. Acta* **75**, 2911–2923.

Stockmann G. J., Wolff-Boenisch D., Gislason S. R. and Oelkers E. H. (2011) Do carbonate precipitates affect dissolution kinetics? 1. Basaltic glass. *Chem. Geol.* **284**, 306–316.

Urosevic M., Rodriguez-Navarro C., Putnis C. V., Cardell C., Putnis A. and Ruiz-Agudo E. (2012) In situ nanoscale observations of the dissolution of $(10\bar{1}4)$ dolomite cleavage surfaces. *Geochim. Cosmochim. Acta* **80**, 1–13.

Vavouraki A. I., Putnis C. V., Putnis A. and Koutsoukos. P. G. (2010) Crystal growth and dissolution of calcite in the presence of fluoride ions: an atomic force microscopy study. *Cryst. Growth Des.* **10**, 60–69.

Wang L. J. and Nancollas G. H. (2008) Calcium Orthophosphates: crystallisation and dissolution. *Chem. Rev.* **108**, 4628–4669.

Wang L. J., Ruiz-Agudo E., Putnis C. V., Menneken M. and Putnis A. (2012a) Kinetics of calcium phosphate nucleation and growth on calcite: implications for predicting the fate of dissolved phosphate species in alkaline soils. *Environ. Sci. Technol.* **46**, 834–842.

Wang L. J., Li S., Ruiz-Agudo E., Putnis C. V. and Putnis A. (2012b) Posner's cluster revisited: direct imaging of nucleation and growth of nanoscale calcium phosphate clusters at the calcite-water interface. *CrystEngComm*. http://dx.doi.org/10.1039/c2ce25669j.

Associate editor: Roy A. Wogelius